Tunable Hybrid Qubit in a GaAs Double Quantum Dot

Gang Cao,[1,2] Hai-Ou Li,[1,2] Guo-Dong Yu,[1,2] Bao-Chuan Wang,[1,2] Bao-Bao Chen,[1,2] Xiang-Xiang Song,[1,2] Ming Xiao,[1,2,*] Guang-Can Guo,[1,2] Hong-Wen Jiang,[3] Xuedong Hu,[4] and Guo-Ping Guo[1,2,†]

[1]*Key Laboratory of Quantum Information, University of Science and Technology of China, Chinese Academy of Sciences, Hefei 230026, China*

[2]*Synergetic Innovation Center of Quantum Information and Quantum Physics, University of Science and Technology of China, Hefei, Anhui 230026, China*

[3]*Department of Physics and Astronomy, University of California at Los Angeles, Los Angeles, California 90095, USA*

[4]*Department of Physics, University at Buffalo, SUNY, Buffalo, New York 14260, USA*

(Received 4 October 2015; published 25 February 2016)

We experimentally demonstrate a tunable hybrid qubit in a five-electron GaAs double quantum dot. The qubit is encoded in the (1,4) charge regime of the double dot and can be manipulated completely electrically. More importantly, dot anharmonicity leads to quasiparallel energy levels and a new anticrossing, which help preserve quantum coherence of the qubit and yield a useful working point. We have performed Larmor precession and Ramsey fringe experiments near the new working point and find that the qubit decoherence time is significantly improved over a charge qubit. This work shows a new way to encode a semiconductor qubit that is controllable and coherent.

DOI: 10.1103/PhysRevLett.116.086801

The promise of massive computing power from the intrinsic parallelism in a quantum system has driven extensive research activities on spin and charge dynamics in semiconductor nanostructures [1–3]. Over the past decade, significant experimental progress has been achieved in demonstrating coherent manipulation of spin- and charge-based qubits. Specifically, a variety of spin qubits have been shown to have extremely long coherence times, though high-fidelity two-qubit gates remain a difficult technical challenge [4–12]. Charge qubits [13–21], on the other hand, can be manipulated very fast because of the strong electrical interaction, which unfortunately also leads to usually short coherence times. Finding a balance between coherence and maneuverability is thus still an open problem in the pursuit of a scalable solid state quantum computer.

A hybrid qubit [22,23] in a Si/SiGe heterostructure is one of the proposals that attempt to address this issue [24–26]. By encoding into two three-electron states in a double dot that have different spin symmetries, relaxation is suppressed. The qubit states also have extended sweet spots, which reduce the effect of charge-noise-induced dephasing [27–33]. Last, the qubit can be manipulated purely electrically. Recent experiments in SiGe-based devices have clearly shown that hybrid qubits are indeed really fast, and their coherence times are significantly longer than charge qubits [34,35].

An intriguing question for us is whether the hybrid qubit design can be adapted to a GaAs double quantum dot. While as a host material for spin qubits GaAs suffers significantly from all the nuclear spins in the lattice, the fast operation speed of a hybrid qubit may alleviate this problem. The lighter electron mass and simpler band structure in GaAs should definitely help in terms of qubit tunability, as has been shown repeatedly in the past quantum dot research work in GaAs [2].

Here we experimentally demonstrate a single tunable hybrid qubit in a GaAs double quantum dot. By working near the (2,3)-(1,4) instead of the (2,1)-(1,2) charge transition, we succeed in tuning our hybrid qubit to an energy splitting in the microwave frequency range. More importantly, asymmetry and anharmonicity in one of the dots leads to a new anticrossing point between the quasiparallel energy levels of the qubit, yielding a versatile and coherent working point. We have performed both Larmor precession and Ramsey fringe experiments on this qubit and demonstrated that at this new working point the qubit has a T_2^* time on the order of 10 ns, much longer than a normal charge qubit. Our results clearly illustrated how a few-electron system can have high degrees of tunability and quantum coherence and appropriate frequency for qubit control. The simple band structure of GaAs allows us to establish a clear understanding on how our qubit works. Further explorations in a GaAs double dot could also help us clarify the roles played by the various electrical noises such as piezoelectric and polar couplings to phonons. Furthermore, the general understanding of the roles played by level degeneracy and dot deformation can also lead to better qubit designs in other (potentially more coherent) substrate materials such as isotopically purified Si.

The system we study is a conventional gated double dot on a $GaAs/Al_{0.3}Ga_{0.7}As$ heterostructure. Figure 1(a) is a scanning electron microscopy (SEM) image of the device. Together with $H1$ and $H2$ gates, $D1$–$D5$ gates define the double dot, and $Q1$–$Q3$ gates define a quantum point contact (QPC). The QPC works at a 0.2 mV dc bias and acts as a charge sensor for the qubit. With the $D5$ gate

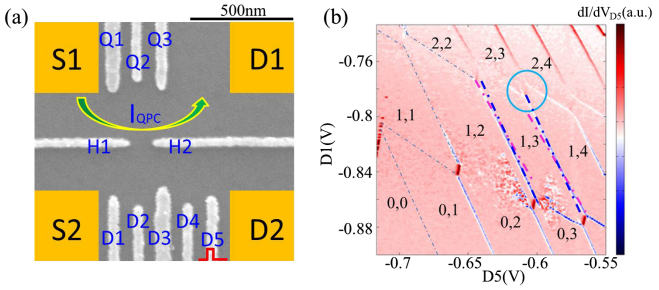

FIG. 1. (a) A SEM image of the sample structure. The density of the 2DEG (95 nm below surface) is 3.2×10^{11} cm^{-2} with a mobility of 1.5×10^5 cm^2/V s. The electron temperature in the device is about 150 mK. (b) Charge diagram of the double quantum dot at $D3 = -0.25$ V, $D4 = -0.35$ V, and $H2 = -0.7$ V. The voltages of gates $D2$ and $H1$ are kept as constant, too. The purple and blue dashed lines present two different charging lines with slopes of -1.68 and -2.17, respectively. To make it clearly visible, the two dashed lines are extended along the charging lines.

determining the energy detuning across the double dot, a particularly interesting quantity is the QPC's transconductance dI/dV_{D5}, which is obtained using a lock-in amplifier and superposing a small ac voltage of amplitude of 0.1 mV on $D5$. Microwave signals can also be applied on gate $D5$, through a semirigid coaxial transmission line from room temperature. We are able to access the few-electron regime for this double dot, as illustrated by the charge stability diagram given in Fig. 1(b).

Denoting the electron numbers in the left and right dots as (N, M), we focus on the low-energy electron dynamics in the region near the (2,3)-(1,4) charge transition for the rest of this Letter. This region is not exactly where the original hybrid qubit works, which was designed near the (2,1)-(1,2) transition. However, since the two core electrons in the right dot occupying the ground orbital state do not participate in the low-energy dynamics at the crossing, the relevant physics is very similar to the three-electron physics between (2,1) and (1,2) configurations. Thus, we will continue to use the three-electron nomenclature to describe the dynamics near the (2,3)-(1,4) crossing [36].

The low-energy sector of the double dot spectrum consists of three five-electron states. Suppose the lowest-energy orbital states in the right dot are ψ_0, ψ_1, and ψ_2. With ψ_0 occupied by the two core electrons, the additional one electron in the right dot in the (2,3) regime will occupy ψ_1, while the additional two electrons in the (1,4) regime will both occupy ψ_1 if they form a singlet or ψ_1 and ψ_2 if they form a triplet state. Thus, near the charge transition there are three relevant low-energy states [36]: $|1\rangle = |S\rangle_L|\uparrow\rangle_R$, $|2\rangle = |\uparrow\rangle_L|S\rangle_R$, and $|3\rangle = (1/\sqrt{3})|\uparrow\rangle_L|T_0\rangle_R - (2/\sqrt{3})|\downarrow\rangle_L|T_\uparrow\rangle_R$, in the $S_z = \frac{1}{2}$ manifold (the $S_z = -\frac{1}{2}$ manifold is degenerate with and decoupled from the $S_z = \frac{1}{2}$ manifold and has identical charge dynamics. However, in the absence of an applied magnetic field, the nuclear spins in the substrate could cause these two manifolds to mix and limits our T_2^* time), identical to those for a hybrid qubit. States $|2\rangle$ and $|3\rangle$ form our hybrid qubit in the (1,4) region, where they are the two lowest-energy states.

Our explorations of charge transitions indicate that different orbital states in the right dot have different charge responses to the applied gate voltages. Figure 2(a) shows the charge stability diagram near the (2,3)-(1,4) transition. Here an additional short pulse of duration $T_p = 300$ ps and magnitude $V_p = 135$ μeV is repeatedly superposed onto the dc sweep of the $D5$ gate [17,18]. Two different sets of charge oscillation peaks can be observed, marked by the blue and purple dashed lines. They clearly have distinct slopes, which indicate that orbital states ψ_1 and ψ_2 (which are the underlying orbital states for states $|2\rangle$ and $|3\rangle$) have different lever arms relative to the $D3$ and $D5$ gates. Consequently, when the gate voltage on the right dot is varied, the energies of states $|2\rangle$ and $|3\rangle$ change differently. In fact, this variation in the response to the applied gate voltages can already be seen in Fig. 1(b), where two different charging lines with slopes -1.68 and -2.17 are marked with purple and blue dashed lines, respectively.

The different responses by ψ_1 and ψ_2 to the applied voltages can be explained by the two states having different "centers of charge," which in turn indicates that the right dot is strongly anharmonic. In a harmonic dot, ψ_1 and ψ_2 would have corresponded to the two degenerate P orbitals of the Fock-Darwin states that are symmetric around the dot center and would have responded to the applied gate voltages in the same manner at the lowest order. In our sample, on the other hand, the double dot energy diagram is shown in Fig. 2(b), where states $|2\rangle$ and $|3\rangle$ are not parallel as functions of the energy detuning. Instead, they cross at a

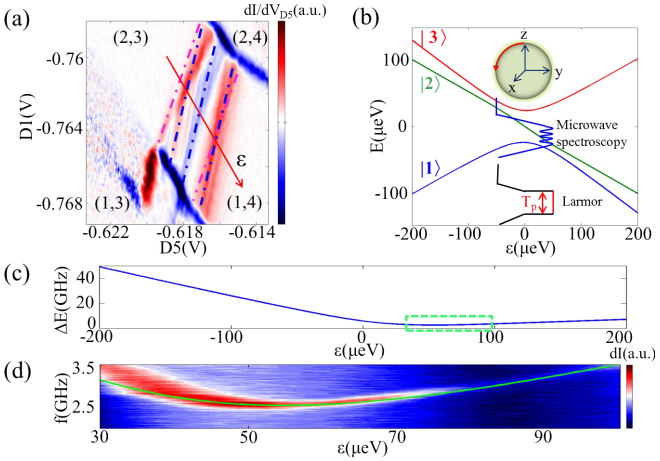

FIG. 2. (a) Charge diagrams under a short pulse $T_p = 300$ ps, $V_p = 135$ μeV at gate voltages of $D3 = -0.217$ V, $D4 = -0.417$ V, and $H2 = -0.717$ V. (b) The simulated energy levels of the system. (c) The energy gap between the ground state and the first excited state in (b). (d) QPC signal as a function of the excitation frequency f of the microwave and the detuning energy. The green line is the energy gap given in the dashed box of (c).

particular detuning, and the crossing becomes an anticrossing after tunnel coupling to the left dot is taken into consideration. Compared with the original hybrid qubit, the Hamiltonian of this three-level system can be written as

$$H = \begin{pmatrix} \varepsilon/2 & \Delta_1 & \Delta_2 \\ \Delta_1 & -\varepsilon/2 & 0 \\ \Delta_2 & 0 & -k\varepsilon/2+\delta \end{pmatrix}. \quad (1)$$

Here ε is the energy detuning between the three states and can be tuned across the interdot charge transition [as shown in Fig. 2(a)], δ is the singlet-triplet splitting within the right dot, and k represents the different lever arms of states $|2\rangle$ and $|3\rangle$. Among the off-diagonal terms are tunnel couplings from $|1\rangle$ to $|2\rangle$ and $|3\rangle$. Direct coupling between $|2\rangle$ and $|3\rangle$ vanishes because of their different spin symmetries.

Instead of having a constant singlet-triplet splitting, states $|2\rangle$ and $|3\rangle$ now have different dependences on the gate voltage, represented by the new phenomenological parameter k for state $|3\rangle$. Since there are two different sets of transition lines mixed with each other in Fig. 2(a), states $|2\rangle$ and $|3\rangle$ should be nearly degenerate at $\varepsilon \sim 0$, which means $\delta \sim 0$. Thus, for simplicity we choose $\delta = 0$ in our calculations. Figure 2(b) shows the energy levels calculated using Eq. (1) with $2\Delta_1 = 9.2$ GHz, $2\Delta_2 = 7.5$ GHz, $k = 1.3$, and $\delta = 0$, while Fig. 2(c) gives the energy splitting between the two lowest levels. States $|2\rangle$ and $|3\rangle$ are not parallel anymore, with level spacing reaching a minimum of ~2.5 GHz at $\varepsilon \sim 55$ μeV.

To verify our model, we characterize the energy levels using microwave spectroscopy [21]. For this and following experiments, a lock-in amplifier's transistor-transistor logic (TTL) signal is used to chop the pulses to generate the sequences, so that half of the TTL period has no pulse, and the lock-in amplifier is also used to measure the QPC's corresponding current change dI [35].

As shown schematically in Fig. 2(b), we initialize our double dot at a negative detuning point, where the ground state, state $|1\rangle$, is nondegenerate and well separated from the excited states. Consequently, our initialization procedure is quite robust. We then increase the detuning adiabatically, over a time period of 10 ns, to the region around the $|2\rangle$–$|3\rangle$ anticrossing. A 20 ns microwave pulse is then applied. Only on resonance can the qubit be excited from the ground state to the excited state. The system is then measured after the detuning is adiabatically lowered in another 10 ns. Figure 2(d) shows the resulting QPC conductance signal. The resonant line agrees well with the calculated result from Hamiltonian (1) presented in Fig. 2(c).

Figure 2 shows that, compared with the original hybrid qubit [19,21], our qubit has some distinct characteristics. Because of the anharmonicity and asymmetry in the right dot, our single-dot energy levels can be modified by changing the gate voltage, making this hybrid qubit tunable. On the negative side, the almost parallel dispersion of the two hybrid qubit states in the original design (and in Fig. S1 of [36]) becomes a nonparallel dispersion when we adjust $D3$ gate voltage, which potentially weakens the qubit against decoherence effects of the environmental charge noise. Considering that hybrid qubit was designed to suppress effects of charge noise by employing parallel energy levels [35,37], it is crucial to clarify the coherence properties of our variant. Below, we explore how the changes of our qubit, particularly the nonparallel energy levels, affect its coherence.

We measure Larmor oscillations and Ramsey fringes near the working point of our hybrid qubit in order to characterize its decoherence. As in the microwave spectroscopy experiment, we initialize the qubit in the ground state $|1\rangle$ in the (2,3) region at $\varepsilon \sim -55$ μeV. We then take the qubit to $\varepsilon \sim 0$ adiabatically using a pulse with a rise time of 3 ns, as shown in Fig. 2(b). The system remains in the ground state. We then apply a nonadiabatic pulse to drive the qubit to $\varepsilon \sim 55$ μeV, deep in the (1,4) region, where the qubit will evolve freely, like the Larmor precession of a spin in a magnetic field, with the excited state acquiring an additional phase relative to the ground state that is proportional to the pulse width T_p. After this free evolution at $\varepsilon \sim 55$ μeV, the detuning is returned nonadiabatically to $\varepsilon \sim 0$ and then adiabatically to $\varepsilon \sim -55$ μeV in 2 ns, at which point we measure the QPC current. If the qubit has evolved to the ground (first excited) state at $\varepsilon \sim 55$ μeV, it would be in $|1\rangle$ ($|2\rangle$) at the end of the pulse sequence. Since states $|1\rangle$ and $|2\rangle$ have different numbers of electrons in the left dot, they can be differentiated by the QPC.

Figure 3(a) shows the results of Larmor precession of the qubit as a function of the pulse width T_p at detuning

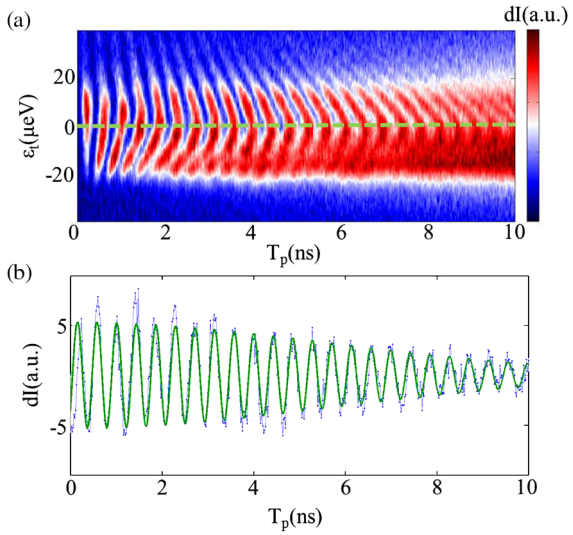

FIG. 3. (a) The Larmor precession and the associated charge oscillations as a function of the nonadiabatic pulse width T_p and ε_t. The signal along the green dashed line is plotted in (b) with blue, while the green solid line is a numerical fit after subtraction of the background and yields a dephasing time of $T_2^* = 8.10$ ns.

$\varepsilon \sim 55$ μeV, or where $\varepsilon_t \sim 0$ (ε_t is defined as the energy detuning relative to the new anticrossing point between the qubit levels). The minimum energy gap at $\varepsilon_t = 0$ is obtained from the oscillation frequency of $2\Delta = 2.43$ GHz, which is consistent with the minimum frequency we extract from Fig. 2(d) using microwave spectroscopy. Figure 3(b) is a cut along the green dashed line in Fig. 3(a), at $\varepsilon_t \sim 0$. Fitting the curve using $A\exp[-(t-t_0)^2/T_2^{*2}]\cos(\omega t+\theta)$, we obtain $T_2^* = 8.10$ ns. This decoherence time is much longer than the value we obtained in the charge qubit regime [36] and values obtained in other charge qubit experiments [13,19,20].

This significant increase in decoherence time originates from the anticrossing of the quasiparallel energy levels in Fig. 2(c). Specifically, the anticrossing and the corresponding optimal point suppresses the charge-noise-induced dephasing. Furthermore, the different spin symmetries of the qubit states suppress the qubit relaxation. Therefore, even though our qubit has lost some of the coherence-preserving ability of the original hybrid qubit design, it still possesses much better coherence properties than an ordinary charge qubit. Moreover, compared with the original hybrid qubit, the new anticrossing point of this qubit, which resides completely in the (1,4) charge region, enables x-axis rotations on the Bloch sphere with a long coherence time.

We have also performed a Ramsey-fringe experiment to further clarify the coherence properties of our qubit in the vicinity of the anticrossing point at $\varepsilon_t \sim 0$. Figure 4(a) presents the pulse shape of the Ramsey experiment, which consists of a free evolution around the z axis in between two $3\pi/2$ rotations around the x axis. Varying the amplitude V_t of the middle pulse between the two x rotations allows the qubit to reach different detuning points.

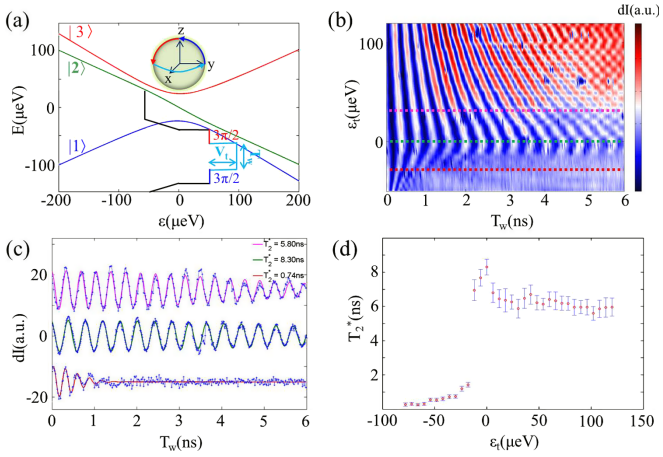

FIG. 4. (a) The simulated energy levels and the pulse shape of Ramsey fringes. The trajectory segments with different colors on the Bloch sphere correspond to the different parts of the applied pulse with the same colors. (b) Ramsey fringes as a function of the inserted pulse width T_w and amplitude ε_t. After subtraction of the background signal, the three dashed lines at $\varepsilon_t = 30$, 0, and -30 μeV are presented and fitted from top to bottom in (c) with an offset current. (d) The extracted T_2^* as a function of detuning energy ε_t.

Figure 4(b) shows the Ramsey fringes as a function of the free evolution point ε_t and the evolution duration T_w. As expected, the Ramsey fringes decay rapidly, in subnanoseconds, when $\varepsilon_t < 0$ and the qubit is in the charge qubit regime, near the (2,3)-(1,4) charge transition. The different charge distributions of the qubit states lead to fast decoherence due to electrical noises [13,17]. In contrast, when $\varepsilon_t \geq 0$, the qubit is deep in the (1,4) charge region, with both qubit states having similar charge distribution. The slowly increasing energy gap also provides some protection for the qubit against charge noise. As a result, the fringes remain quite visible even beyond 6 ns, and the qubit has a much longer decoherence time than in the $\varepsilon_t < 0$ region. The remaining decoherence is possibly due to hyperfine interaction with nuclear spins and residue effects of the charge noise because our levels are only quasiparallel [38]. Figure 4(c) shows three representative cuts, at $\varepsilon_t = 30$, 0, and -30 μeV from top to bottom, respectively. The corresponding decoherence times T_2^* extracted from the curves are $T_2^* \sim 5.8$, 8.30, and 0.74 ns. Figure 4(d) presents decoherence time T_2^* obtained from Fig. 4(b), as a function of the detuning point ε_t.

We note here that the presence of the new anticrossing point for our hybrid encoding allows qubit operations around both the x and z axis with an enhanced coherence time T_2^* of up to 8.3 ns. This is different from the Si hybrid qubit, where x and z rotations are performed at different interdot detunings, so that they have different coherence times [35]. Furthermore, on the positive detuning side for our system [deeper into the (1,4) charge regime], T_2^* only decreases gradually and slowly due to the quasiparallel energy levels.

In conclusion, we have experimentally demonstrated a tunable hybrid qubit in a five-electron GaAs double quantum dot. Specifically, we show that the qubit is tunable because of an anharmonic and asymmetric quantum dot potential. The qubit energy levels anticross instead of being parallel, yielding a new working point. The nonparallel energy levels make the qubit more susceptible to charge noise, but the new working point gives it a higher degree of tunability. To clarify the controllability and coherence of this new qubit, we have performed Larmor precession and Ramsey fringe experiments. We find the qubit decoherence time is quite long, on the order of 10 ns, when it is deep in the (1,4) charge configuration, much slower than in the regular charge qubit regime.

Our results show that this variant of hybrid qubit in a GaAs double quantum dot is both controllable and coherent and acts as a useful platform to study coherent control in a semiconductor nanostructure. To establish its viability as a practical scalable qubit, more work is needed in establishing high-fidelity gates and to identify the optimal approach for a two-qubit gate. In addition, splitting our right dot into

a double dot could make it even more tunable and could open up new avenues for qubit manipulation.

This work was supported by the NFRP (Grant No. 2011CBA00200), the SPRP of the CAS (Grant No. XDB01030000), and the NNSF (Grants No. 11304301, No. 1575172, No. 61306150, and No. 91421303). X. H. and H.-W. J. acknowledge financial support by U.S. ARO through Grant No. W911NF0910393 and No. W911NF1410346, respectively.

G. C. and H.-O. L. contributed equally to this work.

*Corresponding author.
maaxiao@ustc.edu.cn
†Corresponding author.
gpguo@ustc.edu.cn

[1] D. Loss and D. P. DiVincenzo, Phys. Rev. A **57**, 120 (1998).
[2] R. Hanson, L. P. Kouwenhoven, J. R. Petta, S. Tarucha, and L. M. K. Vandersypen, Rev. Mod. Phys. **79**, 1217 (2007).
[3] C. Kloeffel and D. Loss, Annu. Rev. Condens. Matter Phys. **4**, 51 (2013).
[4] J. R. Petta, A. C. Johnson, J. M. Taylor, E. A. Laird, A. Yacoby, M. D. Lukin, C. M. Marcus, M. P. Hanson, and A. C. Gossard, Science **309**, 2180 (2005).
[5] K. C. Nowack, F. H. L. Koppens, Y. V. Nazarov, and L. M. K. Vandersypen, Science **318**, 1430 (2007).
[6] R. Brunner, Y. S. Shin, T. Obata, M. Pioro-Ladriere, T. Kubo, K. Yoshida, T. Taniyama, Y. Tokura, and S. Tarucha, Phys. Rev. Lett. **107**, 146801 (2011).
[7] M. D. Shulman, O. E. Dial, S. P. Harvey, H. Bluhm, V. Umansky, and A. Yacoby, Science **336**, 202 (2012).
[8] F. Forster, G. Petersen, S. Manus, P. Hanggi, D. Schuh, W. Wegscheider, S. Kohler, and S. Ludwig, Phys. Rev. Lett. **112**, 116803 (2014).
[9] X. J. Hao, R. Ruskov, M. Xiao, C. Tahan, and H. W. Jiang, Nat. Commun. **5**, 3860 (2013).
[10] B. M. Maune, M. G. Borselli, B. Huang, T. D. Ladd, P. W. Deelman, K. S. Holabird, A. A. Kiselev, I. Alvarado-Rodriguez, R. S. Ross, A. E. Schmitz, M. Sokolich, C. A. Watson, M. F. Gyure, and A. T. Hunter, Nature (London) **481**, 344 (2012).
[11] M. Veldhorst, J. C. C. Hwang, C. H. Yang, A. W. Leenstra, B. de Ronde, J. P. Dehollain, J. T. Muhonen, F. E. Hudson, K. M. Itoh, A. Morello, and A. S. Dzurak, Nat. Nanotechnol. **9**, 981 (2014).
[12] M. Veldhorst, C. H. Yang1, J. C. C. Hwang, W. Huang, J. P. Dehollain, J. T. Muhonen, S. Simmons, A. Laucht, F. E. Hudson, K. M. Itoh, A. Morello, and A. S. Dzurak, Nature (London) **526**, 410 (2015).
[13] T. Hayashi, T. Fujisawa, H. D. Cheong, Y. H. Jeong, and Y. Hirayama, Phys. Rev. Lett. **91**, 226804 (2003).
[14] J. R. Petta, A. C. Johnson, C. M. Marcus, M. P. Hanson, and A. C. Gossard, Phys. Rev. Lett. **93**, 186802 (2004).
[15] G. Shinkai, T. Hayashi, T. Ota, and T. Fujisawa, Phys. Rev. Lett. **103**, 056802 (2009).
[16] K. D. Petersson, C. G. Smith, D. Anderson, P. Atkinson, G. A. C. Jones, and D. A. Ritchie, Phys. Rev. Lett. **103**, 016805 (2009).
[17] K. D. Petersson, J. R. Petta, H. Lu, and A. C. Gossard, Phys. Rev. Lett. **105**, 246804 (2010).
[18] G. Cao, H. O. Li, T. Tu, L. Wang, C. Zhou, M. Xiao, G. C. Guo, H. W. Jiang, and G. P. Guo, Nat. Commun. **4**, 1401 (2013).
[19] Z. Shi, C. B. Simmons, D. R. Ward, J. R. Prance, R. T. Mohr, T. S. Koh, J. K. Gamble, X. Wu, D. E. Savage, M. G. Lagally, M. Friesen, S. N. Coppersmith, and M. A. Eriksson, Phys. Rev. B **88**, 075416 (2013).
[20] H. O. Li, G. Cao, G. D. Yu, M. Xiao, G. C. Guo, H. W. Jiang, and G. P. Guo, Nat. Commun. **6**, 7681 (2015).
[21] D. Kim, D. R. Ward, C. B. Simmons, J. K. Gamble, R. Blume-Kohout, E. Nielsen, D. E. Savage, M. G. Lagally, M. Friesen, S. N. Coppersmith, and M. A. Eriksson, Nat. Nanotechnol. **10**, 243 (2015).
[22] T. S. Koh, J. K. Gamble, M. Friesen, M. A. Eriksson, and S. N. Coppersmith, Phys. Rev. Lett. **109**, 250503 (2012).
[23] Z. Shi, C. B. Simmons, J. R. Prance, J. K. Gamble, T. S. Koh, Y. P. Shim, X. D. Hu, D. E. Savage, M. G. Lagally, M. A. Eriksson, M. Friesen, and S. N. Coppersmith, Phys. Rev. Lett. **108**, 140503 (2012).
[24] D. P. DiVincenzo, D. Bacon, J. Kempe, G. Burkard, and K. B. Whaley, Nature (London) **408**, 339 (2000).
[25] L. Gaudreau, G. Granger, A. Kam, G. C. Aers, S. A. Studenikin, P. Zawadzki, M. Pioro-Ladrière, Z. R. Wasilewski, and A. S. Sachrajda, Nat. Phys. **8**, 54 (2012).
[26] J. Medford, J. Beil, J. M. Taylor, E. I. Rashba, H. Lu, A. C. Gossard, and C. M. Marcus, Phys. Rev. Lett. **111**, 050501 (2013).
[27] T. Itakura and Y. Tokura, Phys. Rev. B **67**, 195320 (2003).
[28] S. W. Jung, T. Fujisawa, Y. Hirayama, and Y. H. Jeong, Appl. Phys. Lett. **85**, 768 (2004).
[29] G. Ithier, E. Collin, P. Joyez, P. J. Meeson, D. Vion, D. Esteve, F. Chiarello, A. Shnirman, Y. Makhlin, J. Schriefl, and G. Schön, Phys. Rev. B **72**, 134519 (2005).
[30] M. Pioro-Ladrière, J. H. Davies, A. R. Long, A. S. Sachrajda, L. Gaudreau, P. Zawadzki, J. Lapointe, J. Gupta, Z. Wasilewski, and S. Studenikin, Phys. Rev. B **72**, 115331 (2005).
[31] X. Hu and S. Das Sarma, Phys. Rev. Lett. **96**, 100501 (2006).
[32] G. Ramon and X. Hu, Phys. Rev. B **81**, 045304 (2010).
[33] J. K. Gamble, M. Friesen, S. N. Coppersmith, and X. Hu, Phys. Rev. B **86**, 035302 (2012).
[34] Z. Shi, C. B. Simmons, D. R. Ward, J. R. Prance, X. Wu, T. S. Koh, J. K. Gamble, D. E. Savage, M. G. Lagally, M. Friesen, S. N. Coppersmith, and M. A. Eriksson, Nat. Commun. **5**, 3020 (2014).
[35] D. Kim, Z. Shi, C. B. Simmons, D. R. Ward, J. R. Prance, T. S. Koh, J. K. Gamble, D. E. Savage, M. G. Lagally, M. Friesen, S. N. Coppersmith, and M. A. Eriksson, Nature (London) **511**, 70 (2014).
[36] See Supplemental Material at http://link.aps.org/supplemental/10.1103/PhysRevLett.116.086801 for theoretical details and experimental results which are similar with the original hybrid qubit.
[37] J. Koch, T. M. Yu, J. Gambetta, A. A. Houck, D. I. Schuster, J. Majer, A. Blais, M. H. Devoret, S. M. Girvin, and R. J. Schoelkopf, Phys. Rev. A **76**, 042319 (2007).
[38] J. K. Gamble, M. Friesen, S. N. Coppersmith, and X. Hu, Phys. Rev. B **86**, 035302 (2012).